Geomorphology 475 (2025) 109662

Contents lists available at ScienceDirect

Geomorphology

journal homepage: www.journals.elsevier.com/geomorphology

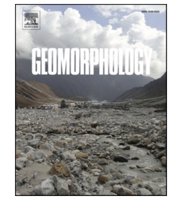

Fault scarps as evidence of historical co-seismic slip - a study of postseismic scarp degradation following the 2016 Norcia earthquake

Robert Elliott [a], Kenneth McCaffrey [a,*], Laura Gregory [b], Luke Wedmore [c]

[a] Department of Earth Sciences, Durham University, Durham, UK
[b] School of Earth & Environment, University of Leeds, Leeds, UK
[c] School of Earth Sciences, University of Bristol, Bristol, UK

ARTICLE INFO

Keywords:
Postseismic
Off Fault Deformation
Afterslip
Erosion
Fault scarp
TLS

ABSTRACT

In immature near-surface normal fault zones, co-seismic slip on a main fault plane will be variably partitioned onto a primary fault scarp and ancillary hanging wall structures and will be subject to ongoing processes of deformation and erosion. The extent to which such processes affect the evidence of visible surface features over time is uncertain, particularly in the first few postseismic years. Using differential repeat Terrestrial Laser Scans (TLS) we investigate continuing postseismic deformation of near-fault areas and degradation in the Monte Vettore region in the Apennines, Central Italy where extensive surface ruptures formed as part of the M_w 6.6 30th October 2016 Norcia earthquake, during the Central Italy Earthquake Sequence ("CIES"), with widely distributed Off Fault Deformation ("OFD"). We concentrate here on one ancillary antithetic structure, the San Lorenzo fault, and the evolution of its scarp over three years following the Norcia earthquake.

The principal causes of postseismic alteration or degradation of fault scarps are expected to be tectonic-related after-slip and/or erosion. Combining careful alignment of repeat TLS, use of an ICP (Iterative Closest Point) algorithm, recursive filtering and detrending techniques, we characterise postseismic surface deformation at ~centimetre scale. We show that afterslip and erosion both play significant roles in the evolution of this fault scarp and the near-fault areas even within the first few postseismic years. Although variable along strike, vertical and horizontal postseismic displacements adjacent to the scarp are ~5–10 % of co-seismic values. Evidence of co-seismic slip associated with such ancillary structures will likely disappear or be significantly degraded quickly relative to the typical earthquake recurrence intervals in the Apennines region, even if the primary fault scarp remains visible. Where fault scarps are used as evidence of previous slip history, particularly in immature fault zones, those factors must be considered to avoid possible misinterpretation of that evidence.

1. Introduction

The accuracy of seismic hazard models depends upon the availability of reliable earthquake records in active tectonic regions. Increasingly, estimates of long-term slip rates are being used to complement seismicity catalogues that are much shorter than the repeat times of earthquakes in a region. Cumulative fault scarps provide records of a succession of earthquakes along the same fault plane (e.g. Wallace, 1977), and pre-date modern remote sensing methods. This longevity is important in areas that have earthquake recurrence intervals of hundreds or thousands of years. Scarps can potentially provide information on the extent of rupture, longer-term tectonic uplift (e.g. Wallace, 1977; Bucknam and Anderson, 1979), the type of slip (e.g. Villani et al., 2018), and the long-term pattern and magnitude of slip (e.g. Papanikolaou et al., 2005; Wei et al., 2021). However, the ability of fault scarps to accurately record the amount of slip in an earthquake can be compromised by (a) the distribution of co-seismic slip between on-fault and near-fault deformation; (b) the extent and nature of afterslip; and (c) geomorphological processes that occur between earthquakes such as weathering or gravitational erosion.

Failure to account for co-seismic Off Fault Deformation (OFD) has been shown to result in significant underestimation of net slip both in field measurements and using remote data (Gold et al., 2021; Scott et al., 2023), particularly in relatively immature fault zones (e.g. Manighetti et al., 2007) where complex deformation patterns are seen (e.g. Milliner et al., 2016; Teran et al., 2015; Burbank and Anderson, 2012;

* Corresponding author.
E-mail address: k.j.w.mccaffrey@durham.ac.uk (K. McCaffrey).

https://doi.org/10.1016/j.geomorph.2025.109662
Received 9 August 2024; Received in revised form 10 February 2025; Accepted 10 February 2025
Available online 12 February 2025

Wesnousky, 1988; Dolan and Haravitch, 2014).

The dominant postseismic tectonic response in the near-field and at shallow depths is expected to be afterslip, possibly associated with poro-elastic rebound, with typical rates of a few millimetres per year (e.g. Riva et al., 2007), orders of magnitude normally smaller than the co-seismic deformation (e.g. Freed et al., 2006), velocity patterns generally inversely proportional to the time since an earthquake (Ingleby and Wright, 2017), and spatially heterogeneic results due to local lithological factors and high gradients in co-seismic slip (Floyd et al., 2016; Cheloni et al., 2010; Wilkinson et al., 2012). Degradation of the fault scarp and its surrounding area due to gravity and weathering will also vary due to factors such as scarp slope angle and areas of steep topography (Hanks et al., 1984; Kokkalas and Koukouvelas, 2005), elevated topography and extreme weather conditions (Wallace, 1977), and differing lithologies (Bucknam and Anderson, 1979, and Wallace, 1980). The degradation will begin and may be most apparent immediately following the scarp's formation when gravitational factors may dominate (Wallace, 1977) and will continue over much longer time periods (potentially indefinitely) (e.g. Nash, 1980).

The Norcia M_w 6.6 earthquake on 30 October 2016 was part of the Central Italy Earthquake Sequence ("CIES") between August 2016 and January 2017 that occurred within the Monte Vettore-Monte Bove region, part of an active extensional region in the Apennines, Central Italy. The Apennines were originally part of a thrust front associated with subduction of the Adria micro-plate beneath the African plate. Westward subduction during the Eocene led to the creation of an accretionary complex, with extension in the Tyrrhenian Basin back arc region (e.g. Jolivet et al., 1998) as the thrust front migrated eastwards towards the Adriatic. The extensional faulting in the Apennines initiated ~2–3 Ma as the thrusting in the Adriatic slowed (Cavinato and De Celles, 1999; Roberts and Michetti, 2004).

Our study examines the postseismic degradation of a fault scarp and its surrounding area on a structure that slipped during the Norcia earthquake. Here, we can investigate the preservation potential of OFD on ancillary structures and can consider the importance of evidence of such structures in any investigation of previous slip history. We investigate the ongoing effects of postseismic processes operating in the near-fault area over nearly 3 years immediately following the Norcia earthquake, with a view to testing the reliability of fault scarps as continuing evidence of co-seismic slip. The study area is an ancillary hanging wall structure that caused a prominent co-seismic surface rupture where none had previously been obvious (although subsequent paleoseismic investigations by Galli et al. (2019) and Cinti et al. (2019) revealed a previous history of ruptures). We look at the various postseismic factors that have resulted in degradation in the area of the ancillary structure even within a short period of time (particularly relative to the long term slip history of the area). We show that both erosion and afterslip played significant roles in the postseismic evolution and degradation of the scarp and its surrounding area.

2. Geological setting

2.1. The Monte Vettore-Monte Bove region, Central Italy

The recent dominant control on the morphology of the Apennines region was glaciation during the last glacial maximum (LGM) in central Italy at ~22,600 years ago (Giraudi and Frezzotti, 1997) and ongoing tectonic activity. The long-term regional extensional faulting has led to a complex array of predominantly northwest-southeast trending and southwest dipping normal faults in the central Apennines region, with fault systems typically in the range of ~20–40 km in length (Galadini and Galli, 2000; Roberts and Michetti, 2004). The faulting shows complex relationships of cross-cutting or reactivation of older structures from previous compressional tectonic phases (e.g. Pizzi and Scisciani, 2000; Pizzi and Galadini, 2009). During the LGM, rates of repeat surface fault slip were matched or exceeded by footwall erosion, leading to fault scarp degradation, or burial with sediment (Roberts and Michetti, 2004). Smooth hillsides formed by periglacial processes are now offset by bedrock fault scarps, which evidence slip over the intervening period (Tucker et al., 2011). The footwalls are formed predominantly from Mesozoic and Tertiary carbonate rocks. Regional slip rates on those faults have been measured at in the region of ~3 mm per year since the demise of the LGM (D'Agostino et al., 2001; Faure Walker et al., 2010), with higher slip rates towards the centre of the array (Roberts and Michetti, 2004).

The Monte Vettore-Monte Bove Fault System ("VBFS") is a complicated NNW-SSE trending fault system located on the northeast flank of the extensional region, in an area of elevated and steep topography, dominated by Monte Vettore, a Mesozoic carbonate ridge which rises to 2476 m above sea level. Winter conditions commonly include significant accumulations of snow. Together with the Laga Mountains Fault System ("LMFS") to the southeast, the VBFS forms the most important extensional fault system in the area. The VBFS and the LMFS are separated by the line of a major regional structure from the previous compressional phase, the Olevano-Antrodoco-Sibillini Thrust ("OAST") (Pierantoni et al., 2013), which trends SSW-NNE in the southern part of the area, juxtaposing Triassic-Miocene (Umbria-Marche) carbonates onto Messinian siliciclastic turbidites of the Laga Formation. The VBFS qualifies as an "immature" system (e.g. criteria applied in Manighetti et al., 2007).

Pre-instrument normal faulting earthquakes in this area include an event of M_w 6.8 in 1703, near the town of Norcia (Galli et al., 2005; Galli et al., 2018). There was no known earthquake of similar magnitude on the Monte Vettore Fault in the historical record (since 1349). However, palaeoseismic investigations suggested it was an active "silent fault" (Galadini and Galli, 2003). Palaeoseismic trenching work at three sites in the Colle Infante and San Lorenzo basin areas (along the antithetic San Lorenzo fault) has revealed 6 surface faulting events (including the CIES) in the past 9 kyr (Galadini and Galli, 2003; Cinti et al., 2019; Galli et al., 2019) and a most recent event at ~1573 years before the CIES.

The topography of the area includes a mixture of steep slopes on Monte Vettore and Monte Bove, and more planar areas, particularly the Pian Grande intra-montane basin to the southwest of Monte Vettore (Fig. 1). Due to the high mountainous terrain, and relatively rapid tectonic uplift, erosion in the area is heavily affected by gravitational factors. Slope deposits and landslide accumulations in the form of scree and loose boulders are present in the hanging wall on most of the west-facing slopes below the main Monte Vettore ridge (Coltorti and Farabollini, 1995), with extensive alluvial deposits and landforms at the base of the mountainside in the Pian Grande area (Pierantoni et al., 2013, Figs. 1 and 2). The bedrock in the Monte Vettore area is almost exclusively Jurassic and Cretaceous limestones and marls, heavily distorted by tectonic activity since the previous glacial maximum.

2.2. The Central Italy earthquake sequence, 2016/17

The CIES between August 2016 and January 2017 affected ~60 km of normal fault system (Pizzi et al., 2017; Villani et al., 2018). The first earthquake in the sequence (Amatrice, M_w 6.2 on 24 August 2016) nucleated at a relay between the VBFS and LMFS. The second, Visso, M_w 5.9, on 26 October 2016, nucleated at a minor relay zone within the north section of the VBFS). The largest magnitude (Norcia, M_w 6.6 on 30 October 2016) involved almost the entire length of the VBFS (Walters et al., 2018). The final main shock (Laga, M_w 5.0–5.5, on 18 January 2017), nucleated within the LMFS. Cross-cutting structures trending SSW-NNE (including the OAST) are thought to have controlled lateral propagation of the ruptures (e.g. Chiaraluce et al., 2017; Pizzi et al., 2017; Walters et al., 2018).

The structures affected by the Norcia earthquake were the main Monte Vettore Fault System ("MVFS") (including ancillary hanging wall structures), and a further structure on the east side of the Pian Grande basin reaching the surface in the Norcia area, generally assumed to be antithetic to the MVFS (e.g. Walters et al., 2018; Cheloni et al., 2019;

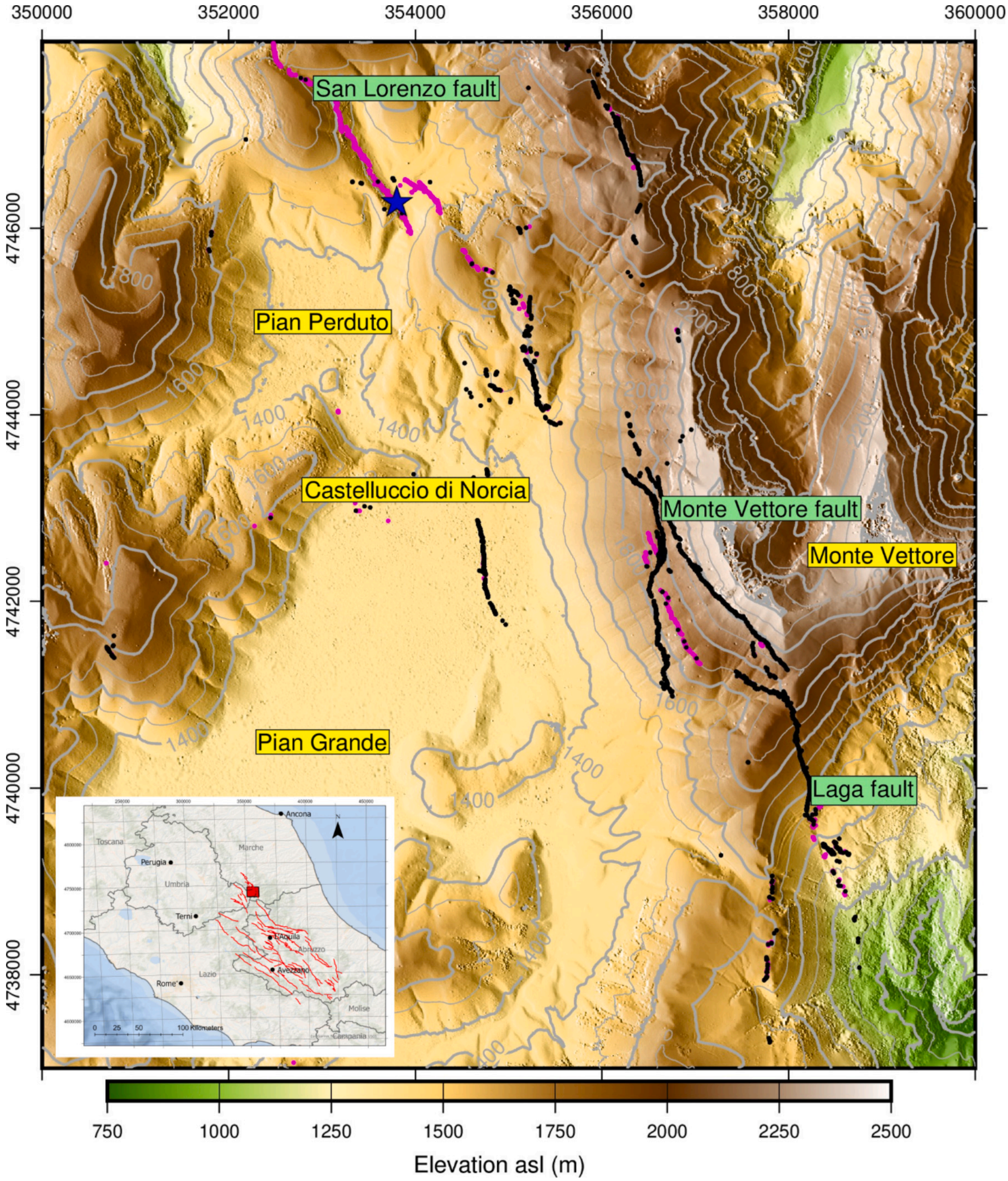

Fig. 1. Area surrounding Monte Vettore, DEM from Pleiades optical satellite data, 1st December 2016. Coordinates are in UTM 33 T. Contours at 100 m intervals. Blue star shows approximate location of San Lorenzo TLS site. Black dots mark locations of synthetic field measurements in 2016/2017, magenta dots antithetic field measurements (from Villani et al., 2018). Inset map The red square shows location of detail in Apennines, Central Italy, with principal faults marked from Fault2SHA Central Apennines Database (Faure Walker et al., https://doi.org/10.1594/PANGAEA.922582).

Chiaraluce et al., 2017).

The Open EMERGEO Working Group compiled an extensive database of co-seismic surface measurements following the Norcia earthquake (Villani et al., 2018, and see locations in study area in Fig. 1). In summary, the field data show southwest-dipping faults, a maximum throw of between 2 m and 2.5 m, a maximum opening of 1 m–1.5 m, and slip vector trend from ~northeast-southwest (~60^0- ~ 240^0). The highest values for co-seismic slip were recorded on the Monte Vettore Fault itself. The co-seismic data also revealed a complex pattern of OFD in the hanging wall of the main Monte Vettore fault (Villani et al., 2018, Fig. 1). One of the sites where surface ruptures were clearly visible was the antithetic San Lorenzo site, shown by the blue star in Figs. 1 and 2.

Using InSAR, Pousse-Beltran et al., 2020 identified postseismic deformation over the 10 weeks period following the Norcia earthquake in the west side of the Pian Grande basin (up to ~1.5 cm - likely to be due to afterslip), and in a smaller region in the vicinity of the postulated reactivation of the OAST near Arquata del Tronto (up to ~5 cm – unlikely to be solely due to afterslip). Mandler et al., 2021 used ground displacement time series from GNSS regional data over a longer timescale (~28 months) and a wider area to identify vertical postseismic movement of up to ~4–5 cm, with a horizontal component of up to ~2 cm towards ~250^0. The probable mechanism for this wider deformation

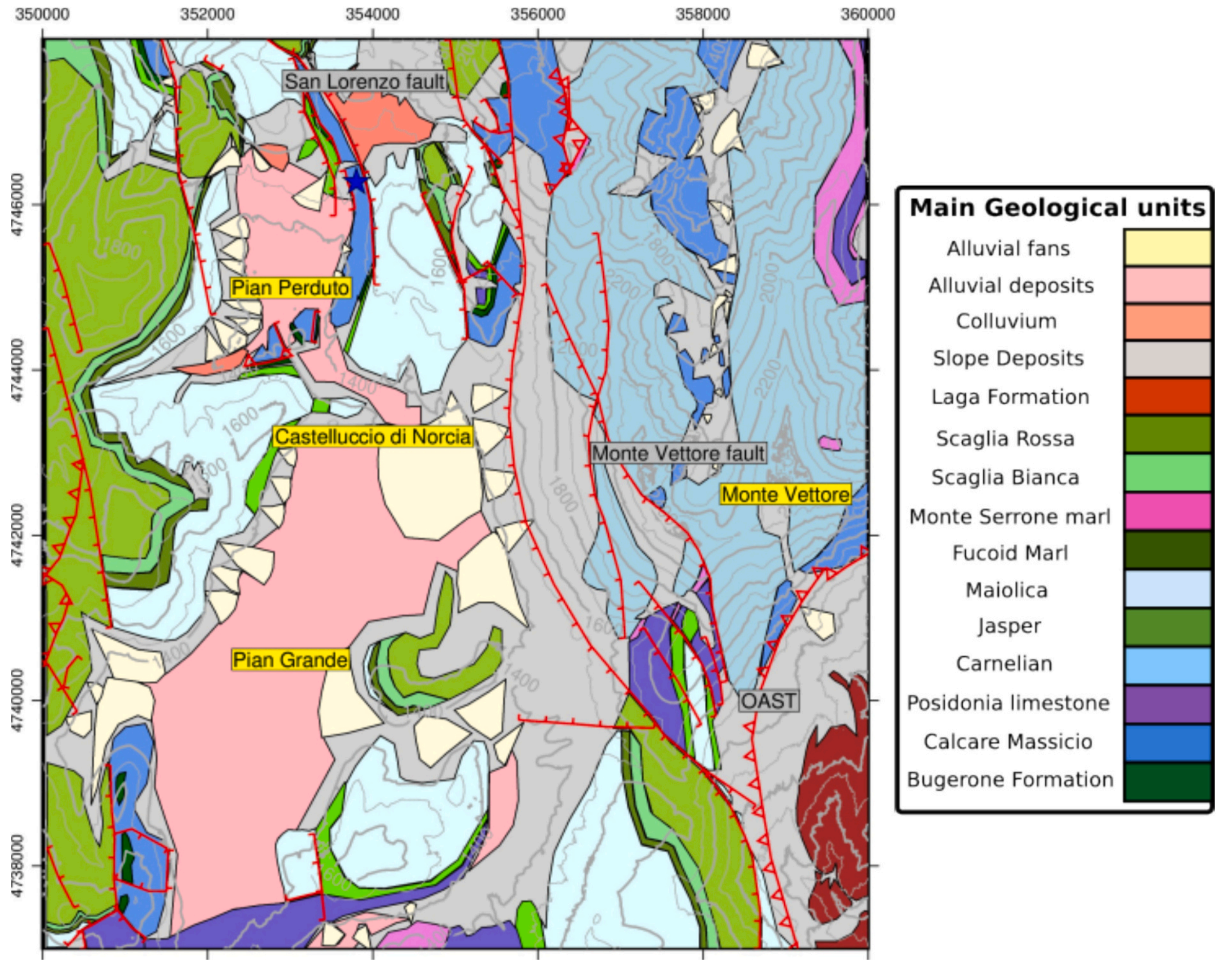

Fig. 2. Simplified Geological map of main Monte Vettore area, adapted from Pierantoni et al., 2013 overlain with contours at 100 m intervals, showing main geological units. Coordinates are in UTM 33 T. Blue star shows approximate location of study site, faults in red.

was thought to be a combination of afterslip and viscoelastic relaxation of the lower crust, with afterslip being the more important process.

3. Method

3.1. Terrestrial laser scanning ("TLS") as an investigatory technique for postseismic slip and geomorphological processes

Following advances in differencing techniques in the last 10 years, airborne LiDAR images acquired by UAVs or aircraft ("ALS") have been used to investigate co-seismic deformation at centimetre to sub-metre scale which is below the resolution of even very high resolution optical satellite data. This has typically been done by comparing ALS results with other datasets. ALS has been used successfully to derive three-dimensional co-seismic displacements by differencing pre-and post-earthquake datasets using ICP algorithms (e.g. Nissen et al., 2014; Nissen et al., 2017; Scott et al., 2018; Lajoie et al., 2019). However, even using ALS, the window sizes required in such techniques to reduce errors may exceed the scale at which the co-seismic deformation is measured (Nissen et al., 2012). Postseismic deformation is expected to be orders of magnitude smaller than the co-seismic deformation (e.g. Freed et al., 2006). Although postseismic deformation may not be confined to the immediate area of the scarp itself, over a period of a few years following a medium-sized earthquake the surface manifestation of such deformation is unlikely to exceed a scale of perhaps a few centimetres (e.g. Wilkinson et al., 2012; Freed et al., 2006).

High-resolution tripod-based TLS scans taken on different occasions have been used successfully in measuring postseismic displacement at millimetre/cm scale (e.g. Wilkinson et al., 2010, Wilkinson et al., 2012, DeLong et al., 2015). They have also been used to measure co-seismic displacement of <20 cm where TLS scans were available from immediately before and after the Norcia earthquake (Wedmore et al., 2019, whose method we use as a starting point for this study), and to investigate landforms associated with co-seismic slip in the 2010 M_w 7.2 El Mayor Cucapeh earthquake using results from scans taken a couple of weeks after the earthquake (Gold et al., 2013).

3.2. The San Lorenzo antithetic fault site

We use a differential TLS approach to assess how erosion and post-seismic deformation can affect preservation of the cumulative record of slip on a fault scarp in space and time. The TLS data were obtained on multiple visits over 3 years at various fault scarp sites which saw co-seismic surface deformation in the Norcia earthquake.

One of these sites is the San Lorenzo antithetic fault, shown on Figs. 1 and 2 by a blue star, at Colle Vinto at 353863, 4746138 UTM 33 T. This hillside sloping site faces NNE, with measured co-seismic antithetic slip towards the northeast (Fig. 3). It is reasonably accessible from a nearby track and results are reported here because the site shows the least anthropogenic modification. Scans were taken of this site on 2nd November 2016 (only 2 days after the Norcia earthquake), 6th October 2017, and 27th August 2019. The site was revisited in May 2022 in order to observe developments since 2019, but only photographs were taken on that occasion.

Fig. 3. San Lorenzo antithetic fault site at 353863, 4746138 UTM 33 T, photograph taken on 29th August 2019, looking southwest. Scale is ~150 m across. Fault scarp visible as thin pale line at base of carbonate outcrops.

The scanner position used for the three scans was placed on raised ground c. 50 m to the NE of the scarp. A slope of limestone bedrock with some scree faces two lower raised areas across a drainage channel. The Pierantoni et al., 2013 geological map records the units as respectively Calcare Massiccio (massive limestone on the hillside) and Eluvium/ Colluvium cover or slope deposits (Fig. 2). Previous faulting appears to have been mapped in the Pierantoni map as an assumed antithetic fault following the line of the foot of the main slope, part of wider antithetic faulting trending ~335^0. Historical Google Earth images prior to the Norcia earthquake do not show any obvious visible fault scarp at this point, although a break in slope is apparent.

The trend of this section of the fault scarp is predominantly southeast-northwest. A prominent feature is a sub-vertical ~4 m high crag at ~50 m from the left-hand edge of Fig. 3 (below a small tree) The hanging wall area to the east of this crag contains larger individual rock fragments of >25 cm × 25 cm which appear to have been detached from the footwall bedrock. Elsewhere further north the hanging wall debris consists of much smaller scale rock fragments of ~5 cm–10 cm length, or light scree.

3.3. Scan processing and differencing

Prior to differencing, the scans were initially cleaned to remove noise from scan returns and multiple scans were co-registered internally. The point clouds from the scans were then filtered using a spatial filter in the Open Source CloudCompare software (CloudCompare v2.10.2) to remove points closer than 2 cm to each other to achieve equivalent resolutions, and reduce the point clouds to manageable size.

Using the CloudCompare rough alignment tool and tie points in each of the pairs of scans, we aligned the 2016 and 2017 scan point clouds more precisely to the coordinates of the 2019 reference cloud by a rigid transformation. Once roughly aligned, where appropriate we aimed to use the point-to-point ICP (iterative closest point) algorithm within CloudCompare to precisely reference the later point cloud in each pair of point clouds to the earlier point cloud using a nearest neighbour comparison, making allowances for the respective degrees of overlap between the point cloud pairs. Ideally, this “fine registration” should be done by identifying a patch common to both point clouds that has not changed between the dates the scans were taken, using the results from that area to apply a transformation to the whole later cloud. In a coseismic situation this would typically be done by identifying a patch of the footwall, deriving the rigid transformation necessary to register that part of the later cloud to the earlier cloud equivalent, and then applying the same transformation to the whole of the later cloud (e.g. Wedmore et al., 2019). However, the user guide to the CloudCompare software (https://www.cloudcompare.org/doc/wiki/index.php/Align) suggests that the ICP registration tool may not work when the clouds have significant differences between them, and in that case fine alignment might not be appropriate. Fine alignment may therefore not be appropriate in postseismic situations where ongoing erosional changes may affect both the footwall and hanging wall. We found that patches of the footwall had altered significantly over the time periods involved. Therefore, fine alignment for the 2016 and 2017 scan pairing was achieved using the whole scans rather than an identified footwall patch. The differences between the 2017 and 2019 scans were such that fine alignment introduced distortion, and we used instead the scans which had been aligned initially using tie points without fine alignment.

We then differenced the respective pairs of aligned point clouds using a windowed point-to-plane ICP algorithm as a method of deriving a “3D” differencing result. This single process yields east-west, north-south and vertical components (Bouaziz et al., 2013; Chen and Medioni, 1992; Nissen et al., 2012; Nissen et al., 2017). We used local windows of 1 m × 1 m, with a buffer zone or fringe of 0.4 m to allow for horizontal displacement (larger than the expected maximum postseismic deformation where the maximum co-seismic deformation recorded in the field was ~1 m), and a sliding window of 0.2 m (adjacent cells overlap by 80 %).

The ICP results contained considerable amounts of noise, especially away from the area immediately adjacent to the fault scarp, with unrealistic values for apparent displacement. After exclusion of results which exceeded 1 m in each of the 3 dimensions, we solved for possible ramps in each dimension to correct for slight variations in scanner alignment by applying a best fit plane correction by way of deduction from the ICP results. These steps removed very little data from the vicinity of the fault scarp, but rather more from the peripheral data (see the Additional Material). Although the results of this selection and detrending clarified the signal, the results remained noisy in places especially for the scan pairing between 2017 and 2019, with anomalous individual results in areas away from the main fault scarp.

We therefore applied a final denoising filtering stage to these 2 scan pairings using a recursive filter applied to a 1 m × 1 m gridded median dataset of the detrended ICP results aiming to replace outliers with median values. The filter uses iterations involving increasing local window sizes from 3 × 3 points up to a maximum of 15 × 15 points (the sequence used was 3, 5, 7, 11, 15). It identifies outlying point values within each iteration which fail to meet a threshold set as a maximum variance (here 0.04 or 4 %) between the median of the values in that window and that value (or the preceding window median if it has been replaced in an earlier iteration) and/or a minimum required level of non-NAN values in that window (here 0.4 or 40 %). Those outlying values are replaced by the median value at each recursive stage, unless and until the threshold is no longer passed, or the series of iterations concludes by reaching its maximum window size. We found that these filter settings achieved the best balance between retaining the signal in the near-fault scarp area whilst removing noise from areas more distant from the scanners, or from comparatively horizontal terrain. The extent of the points replaced in this way can also be seen in the Additional Material.

4. Results

The co-seismic measurements made by the Open EMERGEO Joint Working Party (Villani et al., 2018) recorded either combined offset or throw of ~30–120 cm along this section of scarp (Fig. 4).

The higher co-seismic values are concentrated at the far northwest end of the scarp (as it bends around towards the WNW), and around the area of the sub-vertical crag. Slip vectors where recorded show slip towards ~045–060^0 (Villani et al., 2018 and Fig. 4).

The results for the postseismic displacement between the scans in 2016 (2nd November) and 2017 (6th October) show a consistent pattern of relative displacement of the footwall, with noisier results in the hanging wall data (Fig. 5, LH panel). Vertical displacement of the hanging wall relative to the footwall is ~3 cm downwards, accompanied by horizontal movement of ~2–4 cm ENE-WSW. The highest values (~4–5 cm) are seen where the scarp bends towards to the WNW at the northwest end of the scarp section.

In the footwall area above the sub-vertical crag (labelled 'Crag' on Fig. 5) there is little displacement, although there is ~5 cm horizontal movement towards the NNE ~3 m away from the scarp. In the hanging wall below the crag any horizontal movement also trends largely towards the northeast. Downwards displacement (~2–3 cm) occurs in the area immediately beneath the crag, and over an area extending towards the ENE.

In contrast, the vertical displacement between the scans from 2017 (6th October) and 2019 (26th August) (Fig. 5, RH panel) in areas away from the crag is concentrated in the central part of the scarp, where there is relative downwards displacement of the hanging wall of ~2–4 cm within 2–3 m of the scarp.

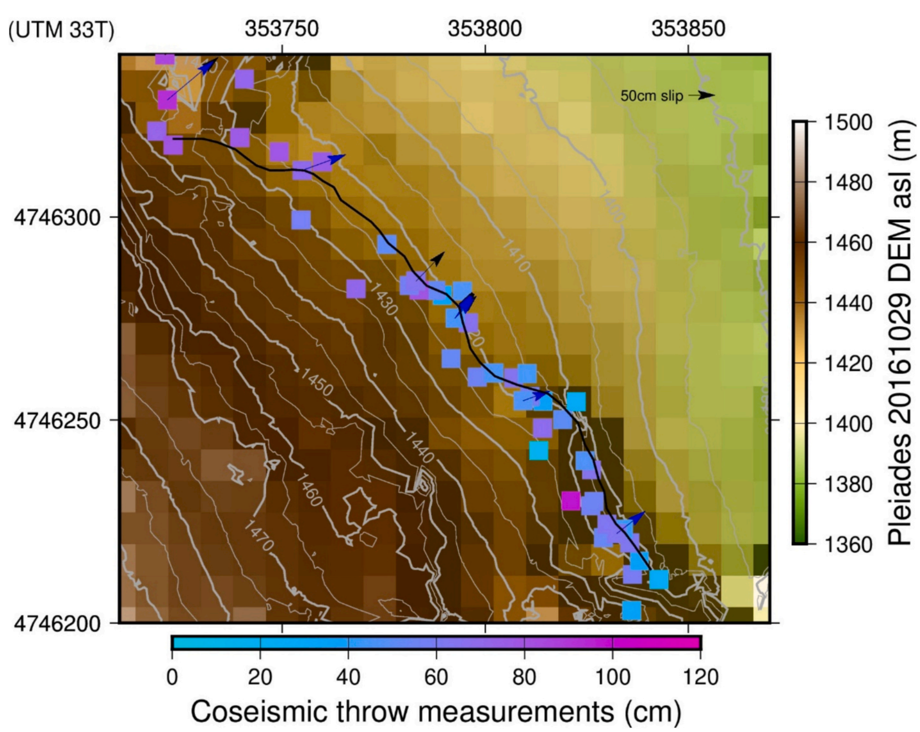

Fig. 4. Co-seismic field measurements, from Villani et al., 2018. Throw measurements are shown by square symbols. Where both slip direction and offset were recorded slip vectors are shown with black arrows. Where slip direction, throw and opening have all been recorded vectors are shown with blue arrows. Background DEM is from Pleiades optical satellite data, from 29th October 2016, adjusted to match TLS coordinates. Approximate fault scarp trace in black line drawn in ArcGIS Pro using DEM, Google Earth and photographs as guides (also used in Figs. 5, 6 and 7).

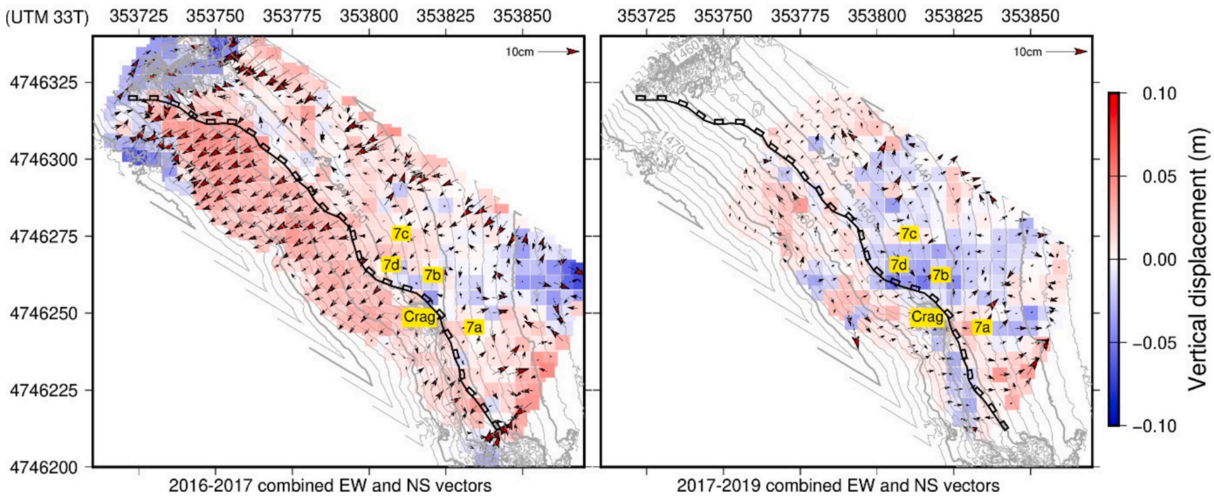

Fig. 5. Median displacement gridded at 5 m × 5 m showing horizontal displacement vectors (arrows) against vertical displacement (background colours) between the 2016 and 2017 scans (LH panel) and 2017 and 2019 scans (RH panel). Contours at intervals of 2 m, from DEM derived from 2nd November 2016 scan. Values at the edge of the data are masked by limiting to movement of +/− 10 cm, to exclude clearly erroneous values from an edge effect. The "Crag" label shows the approximate location of the sub-vertical crag referred to in the text. Labels 7a to 7d show approximate locations of photographs in Fig. 7.

The greatest vertical displacement is particularly apparent to the immediate northwest of the crag (where typically the lowest co-seismic results were recorded, Fig. 4), with lower values further away from the scarp and this area. Note that the 2019 scan did not extend far enough to cover all the area to the northwest of this section.

Profiles through the data from three areas to the northwest of the crag (Fig. 6(a) to (c), centre panels) show the general consistent pattern of displacement between 2016 and 2017. They also highlight in two areas a sharp horizontal displacement of ~4–5 cm from SW to NE in the immediate vicinity of the scarp in that period.

Between 2017 and 2019 the greatest amount of vertical slip is in the central portion of the scarp to the immediate northwest of the crag (Fig. 6(c)). A mean profile across the central part of the scarp in this area shows vertical movement of ~3 cm between 2017 and 2019 accompanied by relative northeast-southwest horizontal displacement of ~2–3 cm within 2–3 m of the scarp (orthogonal to the scarp). The recorded co-seismic slip at this part of the fault scarp was ~50 cm, with similar orientation. The horizontal displacement in this period is largely confined to the hanging wall, with a slight NE trend of ~1–2 cm apparent in each of these profiles.

A profile of the data for the area below the crag and to the east in the hanging wall (Fig. 6(d)), also shows a concentrated area of SW-NE displacement of ~3–4 cm between 2016 and 2017 in the immediate vicinity of the scarp. Vertical displacement in that period is negligible, possibly ~1-2 cm at ~10 m from the scarp.

For the period between 2017 and 2019 the displacement here is significantly different. The main feature is the deposit of material in the hanging wall and erosion of the footwall. In this period debris accumulated over an area of up to ~20 m from the scarp, with up to 3 cm accumulating in the area ~ 6 m from the scarp (Fig. 6(d), RH panel). This feature is not seen either in the 2016–2017 results for this area, or further to the northwest. Here, the footwall is steeper in profile than elsewhere along the scarp and appears less stable. It may be that most loose footwall material had been dislodged co-seismically as a result of shaking. The profile suggests that the footwall is eroding immediately above the scarp in this area (borne out by field photos from May 2022, see Fig. 7 (a) and (b) and the Additional Material).

5. Discussion

The possible causes of postseismic evolution can be grouped broadly into two main types: those related to the tectonic after-effects of the earthquake itself, and those which are external to the earthquake, such as erosion and gravity. Our results from the San Lorenzo antithetic site show that both types played roles in the evolution of the scarp resulting in an increase of the scarp by up to 5–10 % of the co-seismic slip, but significant degradation of the scarp and its surrounding areas within a period of only a few years since the Norcia earthquake. We discuss the controls on the extent and nature of scarp evolutionary and suggest they are due to co-seismic slip gradients, variations in host rock competence and slope gradient.

Much of the postseismic slip follows the expected after-slip pattern for an antithetic structure displaying a continuation of the downwards and northeast-wards movement of the hanging wall side relative to the footwall, which reduces in size over time and with distance from the fault. Models suggest that the decay in the rate of slip should be exponential over time (e.g. Marone et al., 1991, and Zhou et al., 2018). Other observations at this scale also show decay in the extent of slip with distance from the fault (e.g. Wilkinson et al., 2010 and 2012).

Away from the far southeast end of the site where the deformation pattern seems to be heavily influenced by gravitational erosion, the relative vertical displacement between the 2016 and 2017 scans is ~3 cm either side of the scarp, and ~ 1–2 cm downwards further away in the hanging wall (Fig. 6(a) – (c)). The difference in continuing slip between 2017 and 2019 between central portion of the scarp to the immediate northwest of the crag (Fig. 6(c)) (where slip is greatest) and further towards the northwestern end of the scarp (where slip has largely stopped) (e.g. Fig. 6(b)) bears an inverse relationship to co-seismic slip. This suggests that this difference is governed by a co-seismic slip deficit gradient (e.g. Cheloni et al., 2010; Wilkinson et al., 2012). Afterslip appears to have slowed (and possibly stopped) by 2019. This is probably a reflection of the relatively shallow down dip extent of this antithetic structure, which is unlikely to have accumulated a significant amount of co-seismic slip deficit.

Previous studies of postseismic deformation associated with the Norcia earthquake largely discounted poro-elastic rebound (Pousse-Beltran et al., 2020; Mandler et al., 2021). The predominant cause of postseismic slip of some ~4–5 cm in two areas to the south of Monte Vettore and bounded by the OAST, and towards the west side of Pian Grande was thought to be afterslip, largely following the predicted pattern of logarithmic decay over time (Pousse-Beltran et al., 2020, citing the models of Marone et al., 1991 and Zhou et al., 2018). Although generally thought to apply over a longer time scale and larger area, viscoelastic relaxation of the lower crust was not ruled out as a possible

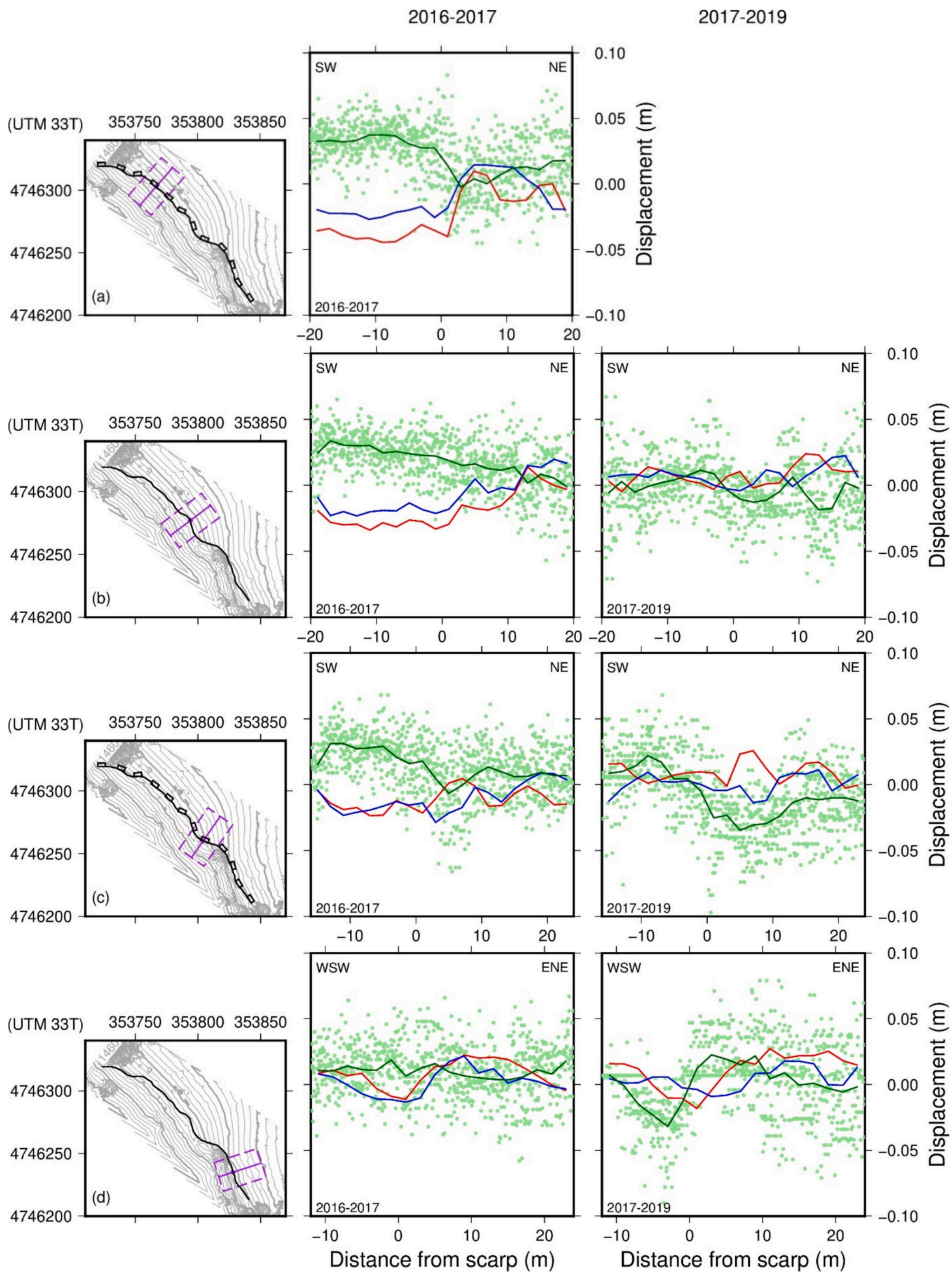

Fig. 6. Profiles of mean vector data, in descending order from northwest to southeast. Locations of data used in calculating means are shown in the dashed magenta box in smaller left-hand panels with data taken from 12 m either side of continuous magenta line. The results panels show mean values for datapoints for east-west (red line), north-south (blue line) and vertical (green line) displacement. Green dots are individual vertical datapoints.

contributory mechanism (Mandler et al., 2021). In the case of the area bounded by the OAST, afterslip might have been triggered in response to heterogeneities in pore fluid pressure arising from the juxtaposition of differing rock units (Pousse-Beltran et al., 2020).

The effects of afterslip in this location are relatively short-lived and restrained, but nevertheless measurable. Afterslip seems largely localised within a few metres of the scarp, and at values which represent ~5–10 % of the co-seismic slip. The San Lorenzo site did not apparently rupture during the preceding Amatrice and Visso earthquakes. However, although co-seismic offset was recorded at >50 cm in places, the post-seismic slip is no more than up to ~5 cm. Fault geometry will play a role in limiting afterslip. The San Lorenzo fault is likely to be a steeply

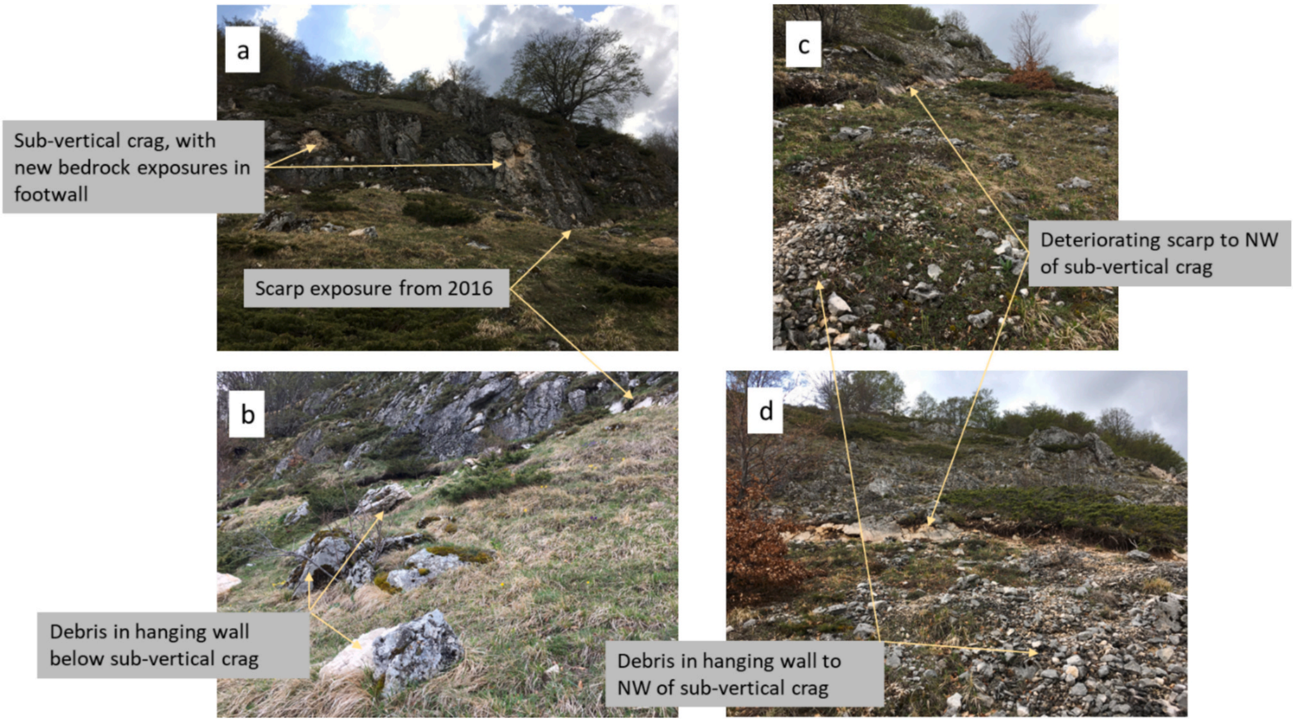

Fig. 7. Field photographs taken on 10th May 2022. (a) shows sub-vertical crag, looking Southwest, (b) shows debris in area below crag looking Southeast, (c) and (d) show degrading sections of the scarp to the Northwest of the outcrop, looking Northwest and West respectively. Locations shown in Fig. 5 above by labels 7a to 7d.

dipping splay originating at relatively shallow depth from a less steeply-dipping synthetic hanging wall structure. That geometry may have limited the extent of slip deficit, and in turn the relatively small amount of afterslip.

Although difficult to compare directly as the timescales and co-seismic displacement are different, the magnitude of the postseimic displacements observed seem to be broadly consistent with the relative magnitude of that observed in relation to the 2009 L'Aquila earthquake (Wilkinson et al., 2012).

In the southeastern area of the scarp beneath the crag (Fig. 6(d)) erosional factors apparently played a significant part from the outset with comparatively little sign of tectonic-related afterslip, except immediately adjacent to the scarp. In this area, the footwall appears to be relatively unstable compared to elsewhere due to its steep gradient. Co-seismic measurements (Villani et al., 2018) indicate that the terrain may be described as “debris”. Over even a relatively short period of time, the consequence of this instability seems to have been the accumulation of a large-scale scree or detached rocks that (in differential TLS results show as mean values calculated over 5 m × 5 m areas) together create a misleading impression of upwards vertical movement of the hanging wall relative to the footwall, particularly since 2017. A comparison of the area involved, using Google Earth images from May 2016 and June 2020 suggests that at least some of the debris in this area pre-dated the CIES (Fig. 8).

On a return visit to the site in May 2022 large segments of rock >25 cm × 25 cm and up to and in excess of ~50 cm × 50 cm had recently become detached from the crag and the footwall immediately next to it (photographs are in Fig. 7(a) and (b) and the Additional Material). If

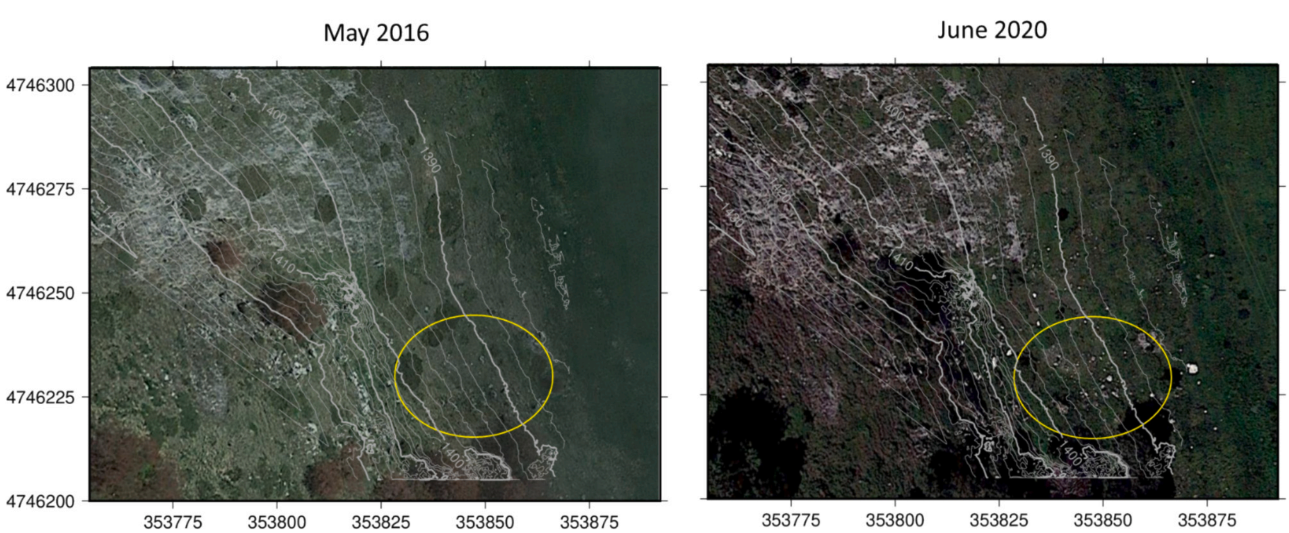

Fig. 8. Google Earth images from May 2016 (LH) and June 2020 (RH) showing in yellow circled area apparent area of larger debris deposition, with contours overlaid from 2nd November 2016 TLS-derived DEM.

loose material is dislodged coseismically, the accumulation of debris between 2017 and 2019 over a wider area suggests that the footwall is eroding immediately above the scarp (which is borne out by field photos from May 2022 – Additional Material). Given this apparent increase in the rate of accumulation in this period and the probable presence of similar debris before the CIES it is unlikely that the process is associated with afterslip. The cause of the increase appears to be larger scree or debris becoming detached from the steep footwall. Away from the crag, other areas of the scarp are now showing signs of rapid degradation through erosion (see photographs in Fig. 7(c) and (d) and the Additional Material).

The previous studies (Pousse-Beltran et al., 2020; Mandler et al., 2021), largely discounted the effects of erosion and gravity. There was no clear link between the topography of the individual locations studied and the deformation observed for gravity to be considered a significant factor (Pousse-Beltran et al., 2020), and the timescales involved (10 weeks after the Norcia earthquake) meant that erosion was unlikely to be a significant factor on its own.

It is unsurprising in an elevated mountainous area with pronounced steep topography that gravitational and weathering erosion play a significant role in scarp degradation (Wallace, 1977; Kokkalas and Koukouvelas, 2005) particularly where freeze-thaw conditions apply over winter (Wallace, 1977). Such erosion would be expected to be most significant in the early period after the scarp formation (Hanks et al., 1984), to which the effect of coseismic shaking could be expected to contribute. Although not necessarily evident from the scans themselves in the ~3 year period since the Norcia earthquake, the rate at which the scarp appears to be eroding at the San Lorenzo site by the time of a return visit in May 2022 suggests that there will be little coherent evidence left of the Norcia earthquake at that site within ~10–20 years. This is one of the consequences of the wide distribution of slip at shallow depths (as is expected to be the case in relatively immature continental earthquake zones, e.g. Milliner et al., 2016, Teran et al., 2015, Gold et al., 2021). Here, erosion is already a significant factor, and will no doubt continue to degrade the remaining scarp and surrounding area. If the widely distributed nature of co-seismic slip is no longer apparent in the evidence preserved in the landscape, then concentrating in the future solely on the "highlights" which remain visible will result in a very distorted picture of the co-seismic slip pattern.

In using fault scarps as evidence of previous seismic slip history, our results show a need to carefully assess the mixture of geology, topography, size distribution and nature of co-seismic slip, and other site-specific factors such as interrelation of faults in order to better understand the processes which have operated on any fault scarp since previous tectonic activity. Our results from this one site illustrate some of the complexities which might arise. Afterslip appears largely to have ceased within 3 years after the Norcia earthquake but gravitational and weathering erosional effects continued. This is an elevated, steep area prone to weathering as well as gravitational factors, with widely distributed co-seismic slip. In such an area, erosion will be the most important factor in assessing the reliability of both the individual scarps and the landforms in the area as a whole, as evidence of previous co-seismic slip. It could be instructive to revisit these sites again over a longer time period to assess the extent to which evidence relating to this and other ancillary structures continues to be degraded, at which stage it might be possible to make a comparison with longer term results and models such as those of Tucker et al., 2011. If the current erosion has been exacerbated by co-seismic shaking, erosion may decrease over time after the initial landscape response.

One consequence of the longer-term degradation of the scarps is that in a few decades, with the exception of possibly the main structures such as the main Monte Vettore Fault, unless there is an intervening tectonic event the surface evidence left of the distributed faulting on minor structures such as the San Lorenzo fault will be increasingly difficult to detect without high resolution data and understanding of morphological processes. This means that possibly <50 % of the co-seismic slip will be clearly recorded in any visible way in the landscape (and the scarps for that remaining element will themselves have deteriorated).

Here, although the results from contemporaneous field observations show a relatively complicated picture of near-fault surface ruptures, it is also likely that slip at depth may be more widely distributed than apparent from co-seismic surface ruptures. Slip on other minor structures may not have fully propagated to the surface in the same way. It has been shown that even relatively major structures in this area including the Norcia Antithetic fault and Pian Piccolo fault did not rupture to the surface (Cheloni et al., 2017; Walters et al., 2018).

Previous use of repeat TLS to derive deformation at similar scales has looked at either less diverse sites (such as roads and relatively flat adjacent areas) over much shorter time periods (e.g. Wilkinson et al., 2010 and 2012), or co-seismic deformation of an order of magnitude greater than the postseismic displacement (e.g. Wedmore et al., 2019). Over those sorts of timescales the sites involved inherently have relatively little gravity-associated or seasonal deformation to complicate the picture. This study applies similar techniques but on a more complex site with more challenging topography over an extended timescale. In any future such exercise consideration could be given to extending further both the size of any area covered and the timescale, although practical constraints may limit the ability to do so.

Some of the workflow is an adaptation of the workflow previously used elsewhere (e.g. Wedmore et al., 2019), such as the use of the scan alignment tools within CloudCompare and the Nissen et al., 2017 modified Iterative Closest Point algorithm. In co-registering scan pairs, the fine alignment process using the CloudCompare tools may need adaptation according to whether it is possible to identify an area which has not changed significantly between scans. The later additions to the workflow here are effectively noise-reducing and reflect the difficulties in extracting a clear signal at these sorts of tolerances and scales from data that could be improved. TLS relies upon returns from objects which may not produce a uniform response depending upon their orientation, and will produce lower returns with distance from the scanner. Scanner set-up is important, as a very small difference in "levelling" the scanners at the outset will produce results which mask the signal. A difference of $\sim 0.01^{0}$ in levelling between scanners will introduce a false vertical difference between the scans of ~1.5–2 cm over a distance of 100 m.

Some of these noise issues could be addressed in the field by taking scans from multiple points and tying them together to avoid some occlusion (e.g. as in Wilkinson et al., 2015). The datasets here were undoubtedly noisy. We found that identifying and removing ramps from the ICP results restored, rather than destroyed, signals. Where the data quality clearly varied significantly with distance away from the fault scarp (as in the 2017–2019 scan pairing) use of the iterative median-based filter allowed replacement of outliers away from the main area, keeping detail near the fault scarp.

6. Conclusion

Although fault scarps preserved in the landscape potentially have an important role to play in the assessment of historic seismic activity, the combined effects of afterslip and erosion in a mountainous area such as the Apennines mean that postseismic processes can severely and rapidly compromise the value of fault scarps as evidence of previous co-seismic slip. In this case the extensive recording of co-seismic deformation and availability of scans from immediately after the Norcia earthquake allows us to track the postseismic changes over 3 years. However, that evidence will not be available for pre-instrumental events, making it difficult to assess the evidential value of what remains preserved in the landscape.

We have investigated a relatively minor structure in the overall partitioning of co-seismic slip. However, taken with other minor structures in the hanging wall of the fault (and structures that may not have ruptured to the surface) those off-fault structures represent a substantial proportion of the co-seismic deformation in an immature fault zone. Slip on the principal fault structures may be the longest-lasting evidence of slip. However as evidence in the form of secondary structures degrades over postseismic time periods of as short as a few years, the remaining evidence preserved in the landscape will increasingly be an unreliable guide as to co-seismic slip.

CRediT authorship contribution statement

Robert Elliott: Writing – original draft, Visualization, Validation, Software, Methodology, Investigation, Formal analysis, Data curation. **Kenneth McCaffrey:** Writing – review & editing, Supervision, Project administration, Methodology, Investigation, Funding acquisition, Conceptualization. **Laura Gregory:** Writing – review & editing, Supervision, Investigation. **Luke Wedmore:** Writing – review & editing, Supervision, Conceptualization.

Funding

This study was part financed by a NERC IAPETUS DTP studentship NE/L002590/1(RE). Data collection immediately post-Norcia earthquake was supported by a NERC Urgency grant (NE/P018858/1).

Declaration of competing interest

I confirm that none of the authors have any competing interests to declare in relation to this manuscript.

Acknowledgements

Richard Walters at the Durham University contributed significantly to the principal author's work as one of his doctoral supervisors, and provided extremely helpful and insightful guidance. However, he is not listed as a co-author of this paper as he left academia before the doctorate was completed, and did not play a role in the drafting of this paper. Tom Phillips, then of the Durham University, provided valuable assistance during the TLS scanning fieldwork in Italy in August 2019. We thank Stéphane Baize and an anonymous reviewer for their helpful and insightful contributions in reviewing this paper.

The majority of the figures have been made using the open source collection of command-line tools Generic Mapping Tools (GMT), version 5.4, Wessel et al., 2013.

Appendix A. Supplementary material

Supplementary material to this article can be found online at http://doi.org/10.15128/r22z10wq246.

Data availability

Data and code available on a **Creative Commons Attribution Non-Commercial** basis at http://doi.org/10.15128/r2dv13zt24r

References

Bouaziz, S., Tagliasacchi, A., Pauly, M., 2013. Sparse iterative closest point. Comp. Graph. Forum 113-123. https://doi.org/10.1145/2988458.2988490.

Bucknam, R.C., Anderson, R.E., 1979. Estimation of fault-scarp ages from a scarp-height-slope-angle relationship. Geology 7, 11–14. https://doi.org/10.1130/0091-7613(1979)7<11:EOFAFA>2.0.CO2.

Burbank, D.W., Anderson, R.S., 2012. Tectonic Geomorphology, 2nd edition. Hoboken, Wiley. https://doi.org/10.2113/gseegeosci.19.2.198.

Cavinato, G.P., De Celles, P.G., 1999. Extensional basins in the tectonically bimodal central Apennines fold-thrust belt, Italy: response to corner flow above a subducting slab in retrograde motion. Geology 27, 955–958. https://doi.org/10.1130/0091-7613(1999)027<0955:EBITTB>2.3.CO2.

Cheloni, D., D'Agostino, N., D'Anastasio, E., Avallone, A., Mantenuto, S., Giuliani, R., Mattone, M., Calcaterra, S., Gambino, P., Dominici, D., Radicioni, F., Fastellini, G., 2010. Co-seismic and initial postseismic slip of the 2009 M_w 6.3 L'Aquila earthquake, Italy, from GPS measurements. Geophys. J. Int. https://doi.org/10.1111/j.1365-246X.2010.04584.x.

Cheloni, D., De Novellis, V., Albano, M., Antonioli, A., Anzidei, M., Atzori, S., Avallone, A., Bignami, C., Bonano, M., Calcaterra, S., Castaldo, R., Casu, F., Cecere, G., De Luca, C., Devoti, R., Di Bucci, D., Esposito, A., Galvani, A., Gambino, P., Giuliani, R., Lanari, R., Manunta, M., Manzo, M., Mattone, M., Montuori, A., Pepe, A., Pepe, S., Pezzo, G., Pietrantonio, G., Polcari, M., Riguzzi, F., Salvi, S., Sepe, V., Serpelloni, E., Solaro, G., Stramondo, S., Tizzani, P., Tolomei, C., Trasatti, E., Valerio, E., Zinno, I., Doglioni, C., 2017. Geodetic model of the 2016 Central Italy earthquake sequence inferred from InSAR and GPS data. Geophys. Res. Lett. 44, 6778–6787. https://doi.org/10.1002/2017GL073580.

Cheloni, D., Falcucci, E., Gori, S., 2019. Half-Graben Rupture Geometry of the 30 October 2016 M_w 6.6 Mt. Vettore-Mt. Bove Earthquake, Central Italy. J. Geophys. Res. Solid Earth 124, 4091–4118. https://doi.org/10.1029/2018JB015851.

Chen, Y., Medioni, G., 1992. Object modelling by registration of multiple range images. Image Vis. Comput. 10, 145–155. https://doi.org/10.1016/0262-8856(92)90066-C.

Chiaraluce, L., Di Stefano, R., Tinti, E., Scognamiglio, M., Michele, M., Casarotti, E., Cattaneo, M., De Gori, P., Chiarabba, C., Monachesi, G., Lombardi, A., Valaroso, L., Latorre, D., Marzorati, S., 2017. The 2016 Central Italy Seismic Sequence: A first look at the Mainshocks, aftershocks, and source models. Seismol. Res. Lett. 88, 757–771. https://doi.org/10.1785/0220160221.

Cinti, F.R., Demartini, P.M, Pantosti, D., Baize, S., Smedile, A., Villani, F., Civico, R., Pucci, R., Lombardi, A.M., Sapia, V., Pizzimenti, L., Caciagli, M., Brunori, C.A., 2019. 22-kyr-Long Record of Surface Faulting Along the Source of the 30 October 2016 Earthquake (Central Apennines, Italy), from integrated paleoseismic data sets. J. Geophys. Res. Solid Earth 124, 9021–9048. https://doi.org/10.1029/2019JB017757.

CLOUDCOMPARE online user guide. https://www.cloudcompare.org/doc/wiki/index.php/Main_Page [Accessed on multiple occasions].

Coltorti, M., Farabollini, P., 1995. Quaternary evolution of the Castelluccio di Norcia Basin. Il Quaternario 8, 149–166.

D'Agostino, N., Giuliani, R., Mattone, M., Bonci, L., 2001. Active crustal extension in the Central Apennines (Italy) inferred from GPS measurements in the interval 1994-1999. Geophys. Res. Lett. 28, 2121–2124. https://doi.org/10.1029/2000GL012462.

DeLong, S.B., Lienkaemper, J.J., Pickering, A.J., Avdievitch, N.N., 2015. Rates and patterns of surface deformation from laser scanning following the South Napa earthquake, California. Geosphere 11, 2015–2030. https://doi.org/10.1130/GES01189.1.

Dolan, J.F., Haravitch, B.D., 2014. How well do surface slip measurements track slip at depth in large strike-slip earthquakes? The importance of fault structural maturity in controlling on-fault slip versus off-fault surface deformation. Earth Planet. Sci. Lett. 388, 38–47. https://doi.org/10.1016/j.epsl.2013.11.043.

Faure Walker, J.P., Roberts, G.P., Sammonds, P.R., Cowie, P., 2010. Comparison of earthquake strains over 102 and 104 year timescales: Insights into variability in the seismic cycle in the central Apennines, Italy. J. Geophys. Res. 115, B10. https://doi.org/10.1029/2009JB006462.

Floyd, M.A., Walters, R.J., Elliott, J.R., Funning, G.J., Svarc, J.L., Murray, J.R., Hooper, A.J., Larsen, Y., Marinkovic, P., Bürgmann, R., Johanson, I.A., Wright, T.J., 2016. Spatial variations in fault friction related to lithology from rupture and afterslip of the 2014 South Napa, California, earthquake. Geophys. Res. Lett. 43, 6808–6816. https://doi.org/10.1002/2016GL069428.

Freed, A.M., Bürgmann, R., Calais, E., Freymueller, J., Hreinsdóttir, S., 2006. Implications of deformation following the 2002 Denali, Alaska, earthquake for postseismic relaxation processes and lithospheric rheology. J. Geophys. Res. 111, B1. https://doi.org/10.1029/2005JB003894.

Galadini, F., Galli, P., 2000. Active Tectonics in the Central Apennines (Italy) – Input Data for Seismic Hazard Assessment. Nat. Hazards 22, 225–268. https://doi.org/10.1023/A:1008149531980.

Galadini, F., Galli, P., 2003. Paleoseismology of silent faults in the Central Apennines (Italy): the Mt. Vettore and Laga Mts. Faults. Ann. Geophys. 46. https://doi.org/10.4401/ag-3457.

Galli, P., Galadini, F., Calzoni, F., 2005. Surface faulting in Norcia (Central Italy): a "paleoseismological perspective". Tectonophysics 403, 117–130. https://doi.org/10.1016/j.tecto.2005.04.003.

Galli, P., Galderisi, A., Ilardo, I., Piscitelli, S., Scionti, V., Bellanova, J., Calzoni, F., 2018. Holocene paleoseismology of the Norcia fault system (Central Italy). Tectonophysics 745, 154–169. https://doi.org/10.1016/j.tecto.2018.08.008.

Galli, P., Galderisi, A., Peronace, E., Giaccio, B., Hajdas, I., Messina, P., Pileggi, D., Polpetta, F., 2019. The Awakening of the Dormant Mount Vettore Fault (2016 Central Italy Earthquake, M_w 6.6): Paleoseismic Clues on its Millennial silences. Tectonics 38, 687–705. https://doi.org/10.1029/2018TC005326.

Giraudi, C., Frezzotti, M., 1997. Late Pleistocene Glacial events in the Central Apennines, Italy. Quat. Res. 48, 280–290. https://doi.org/10.1006/qres.1997.1928.

Gold, P. O., Oskin, M. E., Elliott, A. J., Hinojosa-Corona, A., Taylor, M. H., Kreylos, O. & Cowgill, E. 2013. Co-seismic slip variation assessed from terrestrial lidar scans of the El Mayor–Cucapah surface rupture. Earth Planet. Sci. Lett., 366, 151–162. doi:https://doi.org/10.1016/j.epsl.2013.01.040.

Gold, R.D., Duross, C.B., Barnhart, W.D., 2021. Co-seismic Surface Displacement in the 2019 Ridgecrest Earthquakes: Comparison of Field Measurements and Optical image Correlation results. Geochem. Geophys. Geosyst. 22 (3), e2020GC009326. https://doi.org/10.1029/2020GC009326.

Hanks, T.C., Bucknam, R.C., Lajoie, K.R., Wallace, R.E., 1984. Modification of wave-cut and faulting-controlled landforms. J. Geophys. Res. 89, 5771–5790. https://doi.org/10.1029/JB089iB07p05771.

Ingleby, T., Wright, T.J., 2017. Omori-like decay of postseismic velocities following continental earthquakes. Geophys. Res. Lett. 44, 3119–3130. https://doi.org/10.1002/2017GL072865.
Jolivet, L., Faccenna, C., Goffé, B., Mattei, M., Rossetti, F., Brunet, C., Storti, F., Funiciello, R., Cadet, J.P., D'Agostino, N., Parra, T., 1998. Midcrustal shear zones in postorogenic extension: example from the northern Tyrrhenian Sea. J. Geophys. Res. 103, 12123–12160. https://doi.org/10.1029/97JB03616.
Kokkalas, S., Koukouvelas, I.K., 2005. Fault-scarp degradation modelling in Central Greece: the Kaparelli and Eliki faults (Gulf of Corinth) as a case study. J. Geodyn. 40, 200–215. https://doi.org/10.1016/j.jog.2005.07.006.
Lajoie, L.J., Nissen, E., Johnson, K.L., Arrowsmith, J.R., Glennie, C.L., Hinojosa-Corona, A., Oskin, M.E., 2019. Extent of Low-Angle Normal Slip in the 2010 El Mayor-Cucapah (Mexico) earthquake from Differential Lidar. J. Geophys. Res. Solid Earth 124, 943–956. https://doi.org/10.1029/2018JB016828.
Mandler, E., Pintori, F., Gualandi, A., Anderlini, L., Serpelloni, E., Belardinelli, M.E., 2021. Postseismic Deformation Related to the 2016 Central Italy Seismic Sequence from GPS Displacement Time-Series. Journal of Geophysical Research: Solid. Earth 126 (9), e2021JB022200. https://doi.org/10.1029/2021JB022200.
Manighetti, I., Campillo, M., Bouley, S., Cotton, F., 2007. Earthquake scaling, fault segmentation, and structural maturity. Earth Planet. Sci. Lett. 253, 429–438. https://doi.org/10.1016/j.epsl.2006.11.004.
Marone, C.J., Scholtz, C.H., Bilham, R., 1991. On the mechanics of earthquake afterslip. J. Geophys. Res. 96, 8441–8452. https://doi.org/10.1029/91JB00275.
Milliner, C.W.D., Dolan, J.F., Hollingsworth, J., Leprince, S., Ayoub, F., 2016. Comparison of co-seismic near-field and off-fault surface deformation patterns of the 1992 M_w 7.3 Landers and 1999 M_w 7.1 Hector Mine earthquakes: Implications for controls on the distribution of surface strain: Deformation of Landers and Hector Mine. Geophys. Res. Lett. 43, 10–10,124. https://doi.org/10.1002/2016GL069841.
Nash, D.B., 1980. Morphologic Dating of Degraded Normal Fault Scarps. J. Geol. 88 (3), 353–360. http://www.jstor.org/stable/30062456.
Nissen, E., Krishnan, A.K., Arrowsmith, J.R., Saripalli, S., 2012. Three-dimensional surface displacements and rotations from differencing pre- and post-earthquake LiDAR point clouds. Geophys. Res. Lett. 39 (16). https://doi.org/10.1029/2012GL052460.
Nissen, E., Maruyama, T., Ramon Arrowsmith, J., Elliott, J.R., Krishnan, A.K., Oskin, M. E., Saripalli, S., 2014. Co-seismic fault zone deformation revealed with differential lidar: examples from Japanese Mw ~7 intraplate earthquakes. Earth Planet. Sci. Lett. 405, 244–256. https://doi.org/10.1016/j.epsl.2014.08.031.
Nissen, E., Malireddi, S.R., Clark, K., Hamling, L., Langridge, R., Ries, W., Tagliasacchi, A., 2017. Three-dimensional coastal deformation in the M_w 7.8 Kaikoura earthquake from differential airborne lidar. Proceedings of the 8th International INQUA meeting on Paleoseismology, active Tectonics and Archaeoseismology (Pata). http://web.uvic.ca/~enissen/papers/nissen-etal-2017-PATA.pdf.
Papanikolaou, I. D., Roberts, G. P. & Michetti, A. M. 2005. Fault scarps and deformation rates in Lazio–Abruzzo, Central Italy: Comparison between geological fault slip-rate and GPS data. Tectonophysics, 408, 147–176. doi:https://doi.org/10.1016/j.tecto.2005.05.043.
Pierantoni, P., Deiana, G., Galdenzi, S., 2013. Stratigraphic and structural features of the Sibillini Mountains (Umbria-Marche Apennines, Italy). Ital. J. Geosci. 132, 497–520. https://doi.org/10.3301/IJG.2013.08.
Pizzi, A., Galadini, F., 2009. Pre-existing cross-structures and active fault segmentation in the northern-central Apennines (Italy). Tectonophysics 476, 304–319. https://doi.org/10.1016/j.tecto.2009.03.018.
Pizzi, A. & Scisciani, V. 2000. Methods for determining the Pleistocene–Holocene component of displacement on active faults reactivating pre-Quaternary structures: examples from the Central Apennines (Italy). J. Geodyn., 29, 445–457. doi: https://doi.org/10.1016/S0264-3707(99)00053-8.
Pizzi, A., Di Domenica, A., Gallovič, F., Luzi, L., Puglia, R., 2017. Fault Segmentation as Constraint to the Occurrence of the Main Shocks of the 2016 Central Italy Seismic Sequence. Tectonics 36, 2370–2387. https://doi.org/10.1002/2017TC004652.
Pousse-Beltran, L., Socquet, A., Benedetti, L., Doin, M.P., Rizza, M., D'Agostino, N., 2020. Localized Afterslip at Geometrical Complexities Revealed by InSAR after the 2016 Central Italy Seismic Sequence. Journal of Geophysical Research: Solid. Earth 125 (11), e2019JB019065. https://doi.org/10.1029/2019JB019065.
Riva, R.E.M., Borghi, A., Aoudia, A., Barzaghi, R., Sabadini, R., Panza, G.F., 2007. Viscoelastic relaxation and long-lasting after-slip following the 1997 Umbria-Marche (Central Italy) earthquakes. Geophys. J. Int. 169, 534–546. https://doi.org/10.1111/j.1365-246X.2007.03315.x.
Roberts, G. P. & Michetti, A. M. 2004. Spatial and temporal variations in growth rates along active normal fault systems: an example from The Lazio–Abruzzo Apennines, central Italy. J. Struct. Geol., 26, 339–376. doi:https://doi.org/10.1016/S0191-8141(03)00103-2.
Scott, C.P., Arrowsmith, J.R., Nissen, E., Lajoie, L., Maruyama, T., Chiba, T., 2018. The M 7 2016 Kumamoto, Japan, earthquake: 3-D Deformation along the Fault and within the damage Zone Constrained from Differential Lidar Topography. J. Geophys. Res. Solid Earth 123, 6138–6155. https://doi.org/10.1029/2018JB015581.
Scott, C.P., Adam, R., Arrowsmith, J.R., Madugo, C., Powell, J., Ford, J., Gray, B., Koehler, R., Thompson, S., Sarmiento, A., Dawson, T., Kottke, A., Young, E., Williams, A., Kozaci, O., Oskin, M.E., Burgette, R., Streig, A., Seitz, G., Page, W., Badin, C., Carnes, L., Giblin, J., McNeil, J., Graham, J., Chupik, D., Ingersoll, S., 2023. Evaluating how well active fault mapping predicts earthquake surface-rupture locations. Geosphere 2023 19 (4), 1128–1156. https://doi.org/10.1130/GES02611.1.
Teran, O.J., Fletcher, J.M., Oskin, M.E., Rockwell, T.K., Hudnut, K.W., Spelz, R.M., Akciz, S.O., Hernandez-Flores, A.P., Morelan, A.E., 2015. Geologic and structural controls on rupture zone fabric: A field-based study of the 2010 M_w 7.2 El Mayor-Cucupah earthquake surface rupture. Geosphere 11, 899–920. https://doi.org/10.1130/GES01078.1.
Tucker, E., McCoy, S.W., Whittaker, A.C., Roberts, G.P., Lancaster, S.T., Phillips, R., 2011. Geomorphic significance of postglacial bedrock scarps on normal-fault footwalls. J. Geophys. Res. 116, F01022. https://doi.org/10.1029/2010JF001861.
Villani, F., Civico, R., Pucci, S., Pizzimenti, L., Nappi, R., De Martini, P. M., Agosta, F., Alessio, G., Alfonsi, L., Amanti, M., Amoroso, S., Aringoli, D., Auciello, E., Azzaro, R., Baize, S., Bello, S., Benedetti, L., Bertagnini, A., Binda, G., Bisson, M., Blumetti, A. M., Bonadeo, L., Boncio, P., Bornemann, P., Branca, S., Braun, T., Brozzetti, F., Brunori, C. A., Burrato, P., Caciagli, M., Campobasso, C., Carafa, M., Cinti, F. R., Cirillo, D., Comerci, V., Cucci, L., De Ritis, R., Deiana, G., Del Carlo, P., Del Rio, L., Delorme, A., Di Manna, P., Di Naccio, D., Falconi, L., Falcucci, E., Farabollini, P., Faure Walker, J. P., Ferrarini, F., Ferrario, M. F., Ferry, M., Feuillet, N., Fleury, J., Fracassi, U., Frigerio, C., Galluzzo, F., Gambillara, R., Gaudiosi, G., Goodall, H., Gori, S., Gregory, L. C., Guerrieri, L., Hailemikael, S., Hollingsworth, J., Iezzi, F., Invernizzi, C., Jablonská, D., Jacques, E., Jomard, H., Kastelic, V., Klinger, Y., Lavecchia, G., Leclerc, F., Liberi, F., Lisi, A., Livio, F., Lo Sardo, L., Malet, J. P., Mariucci, M. T., Materazzi, M., Maubant, L., Mazzarini, F., Mccaffrey, K. J. W., Michetti, A. M., Mildon, Z. K., Montone, P., Moro, M., Nave, R., Odin, M., Pace, B., Paggi, S., Pagliuca, N., Pambianchi, G., PantostI, D., Patera, A., Pérouse, E., Pezzo, G., Piccardi, L., Pierantoni, P. P., Pignone, M., Pinzi, S., et al. 2018. A database of the co-seismic effects following the 30 October 2016 Norcia earthquake in Central Italy. (vol 5, 180049, 2018). Sci. Data, 6. doi:https://doi.org/10.1038/sdata.2018.49.
Wallace, R.E., 1977. Profiles and ages of young fault scarps, North-central Nevada. Geol. Soc. Am. Bull. 88, 1267–1281. https://doi.org/10.1130/0016-7606(1977)88<1267:PAAOYF>2.0.CO2.
Wallace, R.E., 1980. Degradation of the Hebgen Lake fault scarps of 1959. Geology 8, 225–229. https://doi.org/10.1130/0091-7613(1980)8<225:DOTHLF>2.0.CO2.
Walters, R.J., Gregory, L.C., Wedmore, L.N.J., Craig, T.J., McCaffrey, K., Wilkinson, M., Chen, J., LI, Z., Elliott, J. R., Goodall, H., Iezzi, F., Livio, F., Michetti, A. M., Roberts, G. & Vittori, E., 2018. Dual control of fault intersections on stop-start rupture in the 2016 Central Italy seismic sequence. Earth Planet. Sci. Lett. 500, 1–14. https://doi.org/10.1016/j.epsl.2018.07.043.
Wedmore, L.N.J., Gregory, L.C., McCaffrey, K.J.W., Goodall, H., Walters, R.J., 2019. Partitioned off-fault deformation in the 2016 Norcia earthquake captured by differential terrestrial laser scanning. Geophys. Res. Lett. 46 (6), 3199–3205. https://doi.org/10.1029/2018GL080858.
Wei, Z., He, H., Lei, Q., Sun, W., Liang, Z., 2021. Constraining co-seismic earthquake slip using Structure from Motion from fault scarp mapping (East Helanshan Fault, China). Geomorphology 375, 107552. https://doi.org/10.1016/j.geomorph.2020.107552.
Wesnousky, S.G., 1988. Seismological and structural evolution of strike-slip faults. Nature 335, 340–343. https://doi.org/10.1038/335340a0.
Wessel, P., Smith, W.H.F., Scharroo, R., Luis, J., Wobbe, F., 2013. Generic Mapping Tools: improved Version Released. Eos 94, 409–410. https://doi.org/10.1002/2013EO450001.
Wilkinson, M., McCaffrey, K.J.W., Roberts, G., Cowie, P.A., Phillips, R.J., Michetti, A.M., Vittori, E., Guerrieri, L., Blumetti, A.M., Bubeck, A., Yates, A., Sileo, G., 2010. Partitioned postseismic deformation associated with the 2009 M_w 6.3 L'Aquila earthquake surface rupture measured using a terrestrial laser scanner. Geophys. Res. Lett. 37 (10). https://doi.org/10.1029/2010GL043099.
Wilkinson, M., Roberts, G.P., McCaffrey, K., Cowie, P.A., Faure Walker, J.P., Papanikolaou, I., Phillips, R.J., Michetti, A.M., Vittori, E., Gregory, L., Wedmore, L., Watson, Z.K., 2015. Slip distributions on active normal faults measured from LiDAR and field mapping of geomorphic offsets: an example from L'Aquila, Italy, and implications for modelling seismic moment release. Geomorphology 237, 130–141. https://doi.org/10.1016/j.geomorph.2014.04.026.
Wilkinson, M.W., McCaffrey, K.J.W., Roberts, G.P., Cowie, P.A., Phillips, R.J., Degasperi, M., Vittori, E., Michetti, A.M., 2012. Distribution and magnitude of postseismic deformation of the 2009 L'Aquila 1 earthquake (M6.3) surface rupture measured using repeat terrestrial laser scanning. Geophys. J. Int. https://doi.org/10.1111/j.1365-246X.2012.05418.x.
Zhou, Y., Thomas, M.Y., Parsons, B., Walker, R., 2018. Time-dependent postseismic slip following the 1978 M 7.3 Tabas-e-Golshan, Iran earthquake revealed by over 20 years of ESA InSAR observations. Earth Planet. Sci. Lett. 483, 64–75. https://doi.org/10.1016/j.epsl.2016.07.038.